第 XX 卷第 XX 期
XXXX 年XX 月

土木与环境工程学报(中英文)
Journal of Civil and Environmental Engineering

Vol. XX No. XX
XX XXXX

DOI: 10.11835/j.issn.2096-6717.2026.032

开放科学(资源服务)标识码OSID:

高海拔密闭增压建筑的耐火性能

李师节[1],王开强[2,3],李国强[4],叶智武[2,3],刘志茂[2,3],刘卫军[2,3],
文康[2,3],张超[1,5]

(1. 武汉大学 土木建筑工程学院,武汉 430072; 2. 中建三局集团有限公司,武汉 430070; 3. 中国建筑先进技术研究院,武汉 430070; 4. 同济大学 土木工程学院,上海 200092;5. 湖北省火灾试验研究中心,武汉 430072)

摘　要:高海拔密闭增压建筑(HAHPB)是一种新型建筑形式,由多个模块化单元组成。通过对舱室内部进行加压和充氧,HAHPB能有效解决高原反应等问题。与普通建筑的基本承重构件不同,HAHPB的基本结构单元是框架钢结构舱室,现有针对普通建筑的防火设计规范难以直接适用于HAHPB。结合HAHPB的建筑功能和结构特点,对比分析防火设计规范确定HAHPB的耐火等级要求,建立HAHPB的有限元模型,采用热-力耦合方法研究HAHPB在不同竖向荷载及舱内外压差工况下、标准火灾条件下的结构温度场演化、应力分布及变形响应,进而确定HAHPB在不同工况下的耐火极限。此外,还通过基于坐标映射的CFD-FEM耦合方法研究HAHPB结构在非均匀受热真实火灾场景下的耐火性能。结果表明,当增压舱内外压差超过0.04MPa时,其耐火极限不能满足要求,需施加防火保护,而在实际密闭火灾工况下,由于火灾持续时间短,结构温升有限,增压舱可不施加防火保护。

关键词:高海拔密闭增压建筑;耐火性能;CFD-FEM耦合;热力行为

中图分类号:TU392.3　　**文献标志码:**A　　**文章编号:**2096-6717(XXXX)XX-0001-17

Fire resistance in high altitude hermetically pressurized buildings

LI Shijie[1], WANG Kaiqiang[2,3], LI Guoqiang[4], YE Zhiwu[2,3], LIU Zhimao[2,3], LIU Weijun[2,3], WEN Kang[2,3], ZHANG Chao[1,5]

(1. School of Civil Engineering, Wuhan University, Wuhan 430072, P. R. China; 2. China Construction Third Engineering Bureau Group Co. LTD, Wuhan 430070, P. R. China; 3. China Construction Institute of Advanced Technology, Wuhan 430070, P. R. China; 4. School of Civil Engineering, Tongji University, Shanghai 200092, P. R. China; 5.Fire Testing and Research Center of Hubei Province, Wuhan 430072, P. R. China)

Abstract: High Altitude Hermetically Pressurized Buildings (HAHPBs) are a new form of construction composed of multiple modular units. By pressurizing and supplementing oxygen within each compartment HAHPBs can effectively address issues such as altitude sickness. Unlike the basic load-bearing components of ordinary buildings, the fundamental structural unit of an HAHPB is a framed steel compartment. Therefore, existing fire safety design codes for ordinary buildings cannot be directly applied to HAHPBs. Based on the building functions and structural characteristics of HAHPBs, this study compares and analyzes fire safety design

Received: 2026-01-16

Foundation item: China Construction Technology Innovation Platform Construction Fund (No. CSCEC-PT-011)

Author brief: LI Shijie (1996-), PhD candidate, main research interest: structural fire engineering, E-mail: scdzlsj@whu.edu.cn.
ZHANG Chao (corresponding author), professor, doctorial supervisor, E-mail: chao.zhang@whu.edu.cn.

codes to determine the required fire resistance rating of HAHPBs. Then, a finite element model of the HAHPB was established, and a thermo-mechanical coupling method was adopted to investigate the structural temperature field evolution, stress distribution, and deformation response under standard fire conditions with different vertical loads and internal-external pressure difference conditions, thereby determining the fire resistance limits under different conditions. Additionally, the fire resistance performance of the HAHPB structure under realistic fire scenarios with non-uniform heating was investigated through a CFD-FEM coupling method based on coordinate mapping. Results show that when the internal-external pressure difference of the pressurized cabin exceeds 0.04 MPa, the fire resistance limit fails to meet the required rating, and fire protection measures become necessary. Under realistic fire scenarios, the temperature rise of the structure is limited because of the short fire duration and the pressurized cabin is able to satisfy the chosen fire resistance requirement without additional fire protection.

Keywords: High altitude hermetically pressurized buildings; Fire resistance; CFD-FEM coupling; Thermo-mechanical behavior

1 Introduction

The Tibetan Plateau, known as the "Roof of the World" and the "Water Tower of Asia," serves as a climate change indicator for Asia and even the rest of the Northern Hemisphere since it exerts significant influence on global climate. China's push to elevate the ecological protection of Tibet to a national strategic level has resulted in a growing number of scientific research teams, workers, and tourists flocking to the region, which has led to rapid development. However, the low oxygen and low atmospheric pressure of the plateau cause altitude sickness for many visitors. To alleviate the symptoms of altitude sickness and provide travelers with a better experience, High Altitude Hermetically Pressurized Buildings (HAHPBs) have been constructed. HAHPBs are a new architectural form composed of multiple modular units, as shown in Figure 1. Each modular unit includes basic modules such as standard compartments, corridors, and transition compartments, and these modules are interconnected through connection nodes. By utilizing pressurization and oxygen supplementation technology within the compartments, HAHPBs can ensure that key human habitation indicators such as atmospheric pressure, oxygen concentration, and temperature and humidity levels within the compartments are equivalent to those near sea level, which can effectively solve altitude sickness problems and related issues[1].

However, one problem with the novelty of HAHPB construction remains: lack of an appropriate fire code. Building fires account for 80% of all fire incidents annually[2]. This is particularly concerning for steel structures, as the strength of steel significantly decreases at high temperatures, leading to structural failure or even collapse in the event of fire. HAHPBs, which are constructed from welded square steel tubes and steel plates, are especially prone to structural damage during a fire. Although HAHPBs must comply with existing fire codes, this may not be sufficient protection given the nature of their construction. Existing codes only specify the fire resistance rating (FRR) requirement for individual components (e. g. beams, slabs, columns, and walls) in ordinary buildings, without giving the FRR requirement for integral load-bearing units like the cabins used in HAHPBs. It is thus essential to determine the required FRR for HAHPBs by analyzing their fire risk, building height, functional use, and importance.

The FRR of structural components is conventionally determined by standard fire tests conducted in furnaces[3-8]. Such tests typically involve isolated components with simple constrained conditions (or no conditions), but actual structures have complex and diverse constraints. Therefore, the performance of the test components typically does not represent the actual performance of entire structures well[9-12]. Furthermore, furnace tests often assume uniform temperature conditions, but real fires typically exhibit nonuniform temperature conditions. Nonuniform gas temperature distribution can cause temperature gradients within structures that lead to uneven expansion, internal force redistribution, and even changes in failure modes[13-14]. For example, theoretical studies have found that both steel beams and steel columns can exhibit different failure modes and lower failure temperatures in localized fires with nonuniform temperature distributions compared to the "standard" fire with uniform temperature[15-17]. The fundamental structural unit of an HAHPB is a framed steel cabin, the size of which often exceeds the limitation of current test furnaces and cannot be subdivided into smaller load-bearing units. As a result, the fire resistance of HAHPBs is difficult to determine through standard fire tests and realistic fire scenarios (with nonuniform temperatures) should be considered in the structural fire design of HAHPB.

In this paper, the fire resistance of an HAHPB is theoretically studied following three steps. First, domestic and international building fire codes (including GB 50016[18], GB 55037[19], GB 50368[20], IBC[21]) are compared and analyzed to establish an initial FRR requirement for HAHPB cabins. Second, a finite element (FE) model of a typical HAHPB cabin is developed to study its FR under various load (pressurization) levels. Finally, the FE model is further used to study the FR of the cabin in a localized fire scenario. A fire dynamics simulator (FDS) is used to model the localized fire behavior, and the FDS-FEM coupling method[22-25] is used to transfer the thermal boundary condition data from the FDS to the FEM. By comparing the mechanical responses of an HAHPB cabin under standard fire and localized fire, suggestions for the FR of the HAHPB are given that may provide a basis for subsequent fire-resistant design and structural optimization.

2 Literature review

2.1 Fire behavior in high-altitude regions

As altitude increases, both atmospheric pressure and oxygen concentration decrease, leading to notable differences in the characteristics and development of fires in high-altitude regions compared to those in lower areas. Studies have shown that with increasing altitude and decreasing atmospheric pressure, combustibles undergo faster pyrolysis and mass loss, making them easier to ignite. This significantly increases the risk of fire of combustible materials in high-altitude locations[26-28]. Current research on fires

Fig.1 High altitude hermetically pressurized buildings

in high-altitude buildings is largely confined to experimental and simulation studies of smoke spread in tunnel fires[29-30], and investigations into residential building fires under low-pressure and low-oxygen conditions remain absent.

The combustible materials inside a pressurized cabin are primarily solid fuels. Studies have shown that the changes in the pyrolysis and ignition characteristics of solid fuels under high-altitude conditions are primarily attributable to low-pressure environments rather than variations in oxygen concentration. Delichatsios[31], through experiments on plywood, found that key parameters such as ignition time, critical heat flux, and critical mass loss rate remained largely unchanged with varying oxygen concentrations, confirming the idea that oxygen concentration has a limited influence on the pyrolysis ignition process. This conclusion is supported by Hirsch et al. [32], whose research also indicates that the critical oxygen concentration required for ignition varies little across different pressures, suggesting that the altered pyrolysis behavior of fuels in high-altitude environments is mainly driven by reduced pressure. In addition, Simulated spacecraft cabin experiments conducted by Fereres et al. [33-34] elucidate the mechanisms by which low pressure significantly reduces ignition time and critical mass flux. Low pressure reduces convective heat loss from the fuel surface, accelerating the pyrolysis process, and the formation of a thick layer of pyrolysis gases and localized low-oxygen conditions under low pressure promotes a gas mixture more prone to ignition. These studies, validated through FDS simulations, not only confirm the dominant role of low pressure but also highlight the fact that the increased fire hazard in high-altitude environments is primarily due to the combined thermodynamic and chemical kinetic effects of reduced pressure, which make solid fuels more likely to reach ignition conditions, greatly increasing the risk of fire initiation and spread.

Through comparative experiments conducted at multiple altitudes, Qie et al. [35] revealed the enhancing effect of low-pressure environments on the pyrolysis and ignition of solid fuels in the presence of an ignition source. Their experiments demonstrate that under the same radiative heat flux, wood and PMMA in high-altitude regions exhibited faster pyrolysis rates and greater ignitability, primarily due to the significant promotion of pyrolysis gas release under low-pressure conditions. Based on existing research, we therefore conclude that in low-pressure environments, the pyrolysis rate of solid fuels generally increases, and the ignition time consistently decreases as pressure drops. This correlation mechanism explains the primary reason for the increased risk of fire in high-altitude regions: by accelerating the pyrolysis process and facilitating the release of combustible gases, low-pressure conditions enable solid fuels to reach ignition thresholds more easily, thereby significantly lowering the energy required for fire initiation.

2.2 FRR requirements

The term fire resistance (FR) refers to the ability of a material or structure to withstand fire. In practice, FR or FRR is defined as the duration of time that an element of building construction is able to withstand exposure to a standard temperature/time and pressure regime without a loss of its fire separating function, load-bearing function, or both[18]. Load-bearing elements in buildings are typically divided into beams, columns, slabs, walls, and roof components, and fire codes specify these elements' FRR requirements accordingly. However, HAHPBs are constructed by accumulation of steel cabins (compartments) that are designed to bear the pressure differences between indoor and outside environments and can't be structurally divided into smaller components.

In the current Chinese fire safety regulations, the Code for Fire Protection Design of Buildings (GB 50016-2014), no specific building category has been established for modular buildings or high-altitude pressurized buildings. Instead, fire protection design is generally determined according to the building's occupancy type. For example, when modular buildings are used for hotel accommodations, they are typically classified as hotel buildings or as hotel-type occupancy within public buildings, and the required FRR and FR limits of structural members are determined based on factors such as building height, number of stories, and building scale. No specific provisions are provided for the fire performance of modular steel structures, and there are also no relevant definitions or FR requirements for structural systems such as pressurized cabins with integral steel frame structures. In contrast, foreign codes provide relatively clearer applicability to modular buildings. For example, although the International Building Code (IBC) also uses a classification system based on occupancy classification, the IBC provides a relatively mature framework for the fire resistance design of steel structures and offers clearer definitions and requirements regarding the FRR and structural fire protection of integrated steel frame structural systems, such as those used in pressurized cabins.

The IBC[21] specifies FRR requirements for primary structural frameworks instead of individual components. Section 202 in the code specifically defines the primary structural framework as: 1) columns; 2) structural components directly connected to columns, including beams, girders, trusses, and braces; 3) components of floor and roof structures directly connected to columns; and 4) components critical to the vertical stability of the primary structural framework under gravity loads. The steel cabins in HAH-

PBs can be described as the primary structural framework under the IBC, and their FRR requirements may thus be determined according to IBC requirements.

2. 3 Effect of temperature gradients

Current structural fire design methods are primarily based on fully developed compartment fires that are characterized by an approximately uniform gas temperature distribution throughout the compartment. However, real fires typically begin as localized combustion, during which the temperature distribution in space is significantly nonuniform. Under actual fire conditions, the internal temperature field of steel structural members is therefore often highly nonuniform as well, with the specific distribution influenced by factors such as the fire source location, member geometry, and boundary conditions. In particular, for steel beams protected by a floor slab on the top side but exposed to standard fire conditions on the other three sides, obvious temperature gradients occur within the cross-section. This nonuniform heating effect has an important impact on the thermal response and structural performance of steel members. [17]

Due to the presence of temperature gradients, the failure or buckling temperature of steel members under localized fire conditions may be significantly lower than that under standard fire conditions [36]. Zhang et al. [16] conducted a numerical study on the structural performance of exposed steel columns subjected to localized fires. They found that when the investigated steel columns were surrounded by localized fire, their buckling temperatures were higher than those under the standard ISO 834 fire. However, when the steel columns were adjacent to localized fire, their buckling temperatures could be significantly lower than those under the standard ISO 834 fire. Usmani et al. [37] also analyzed the influence of linear temperature distribution along the cross-section depth on the load-bearing mechanism of compression members and found that the temperature gradient in the cross-section induced a secondary moment that might lead to unconservative evaluation of loadbearing capacity. Similarly, Tan et al. [38] studied the effect of linear temperature distribution along the column length on buckling behavior of restrained steel columns. They found that the longitudinal temperature gradient could significantly reduce the column's buckling capacity. In other work Scullion et al. [39] experimentally investigated the failure temperatures of axially loaded elliptical hollow steel columns subjected to hydrocarbon fire exposure. The failure temperatures for the investigated steel columns under the hydrocarbon fire condition were significantly lower than the failure temperatures calculated according to the Eurocode[40]. Furthermore, Agarwal et al. [41] experimentally and numerically investigated the impact of through-thickness temperature gradient on fail temperature of steel columns and found that in most investigated cases steel columns with temperature gradients failed at lower average temperatures.

In addition, Zhang et al. [15] numerically investigated the influence of 3D (three-dimensional) nonlinear temperature gradients on the LTB (lateral-torsional buckling) temperature of steel beams under fire conditions. LTB temperature was defined as the maximum temperature in the steel beam when LTB occurred. They found that LTB temperatures under the investigated localized fire conditions could be significantly lower than those under the standard ISO 834 fire condition. Likewise, Yin et al. [42] numerically investigated the influence of temperature gradient on the LTB temperature of steel beams considering both linear and bilinear temperature profiles along the depth of the cross-section. Temperature gradients along the beam length were not considered. The LTB temperatures for the investigated steel beams with temperature gradients were higher than those without temperature gradients. In still other work Dwaikat et al. [43] experimentally studied the effect of cross-section temperature gradients on the performance of steel beam-column members and found that the profile of the temperature gradient significantly influenced the mechanical response of beam-columns. Finally, Possidente et al. [44] recently surveyed recent studies on steel columns subjected to localized fires and suggested that advanced simulation methods should be used to capture the column's thermo-mechanical response more accurately.

2. 4 Research significance

The above literature review shows that there is currently no technical data on the fire performance of steel structures in the high-altitude regions; the current Chinese fire code provides no specification on FRR requirements of integral loadbearing structures such as steel cabins; and temperature gradients in realistic fires might significantly reduce the failure temperatures of steel members, but current design methods are based a standardized fire that assumes uniform heating conditions.

Therefore, to ensure the fire safety of HAHPBs and to understand the failure mechanism of integral loadbearing structures in fires, it is necessary to carry out advanced simulations to study the thermo-mechanical responses of HAHPBs under both standardized and realistic fire conditions.

3 Project overview

3.1 Details of a standard cabin

A HAHPB is composed of multiple modular units, with each unit containing basic modules such as standard cabins, corridor cabins, and transition cabins. This study focuses on a standard HAHPB which has dimensions of 6.3 m in length, 3.7 m in width, and 3.3 m in height, as shown in Figure 2. The HAHPB standard cabin is primarily intended for people who live and work in high-altitude regions for extended periods or those who travel there temporarily for business or tourism, such as engineering and technical personnel, plateau stationed staff, and tourists. The reduction in atmospheric pressure at high altitudes is the fundamental cause of altitude sickness, and a standard HAHPB cabin is primarily designed to serve as a hotel accommodation unit in high-altitude regions, providing a relatively comfortable living environment for individuals traveling or working temporarily at high altitudes, and effectively meeting the accommodation needs of most short-term visitors and staff. In addition, a cabin can also integrate both residential and office functions according to practical needs, such as single- or double-occupancy accommodation units or small office spaces.

The standard cabin investigated in this study is designed based on the typical unit dimensions of modular pressurized high-altitude buildings, specifically standard hotel guest room units. it has a modular steel structural frame, which can be prefabricated in factories and transported to high-altitude regions for rapid on-site installation, thereby accommodating constrained construction conditions and the demand for high construction efficiency in plateau environments. its designed service life is generally considered to be 20-30 years, during which the structure is required to satisfy both structural safety and fire safety requirements.

A standard HAHPB cabin is constructed using Q355 steel plates and two types of welded square steel tubes: B150×150×10 and B120×120×10. The B150×150×10 square steel tubes are primarily positioned at the outer supports and mid-span areas of the frame, as marked by the red line in Figure 2 (b), and the remaining sections employ B120×120×10mm tubes to provide cooperative constraint. The thickness of the steel plates between the steel frames is 5mm, welded to the side of the square steel tubes, concave 5mm inward compared to the outer surface of the steel tubes, as shown in Figure 2(c). In addition to its own gravity load, the upper part of the cabin bears vertical loads ranging from 300 to 1 000 kN, with an internal pressure differential of 0.02 to 0.05 MPa.

Table 1 Building classification requirements

Occupancy classification	Configuration	Allowable building height above grade plane (m)	Configuration	Allowable number of stories above grade plane	Configuration	Allowable area factor (m^2)
R	NS	15.24	NS	3	NS	1114.8
	S13D	15.24	S13R	4	S13R	1114.8
	S13R	18.288	S13R	4	S1	4459.2
	S	21.336	S	4	SM	3344.4

Note: NS: Buildings not equipped throughout with an automatic sprinkler system. S13D: Buildings equipped throughout with an automatic sprinkler system in accordance with NFPA 13D. S13R: Buildings equipped throughout with an automatic sprinkler system in accordance with NFPA 13R. S: Buildings equipped throughout with an automatic sprinkler system. S1: Buildings a maximum of one story above grade equipped throughout with an automatic sprinkler system. SM: Buildings two or more stories above grade plane equipped throughout with an automatic sprinkler system.

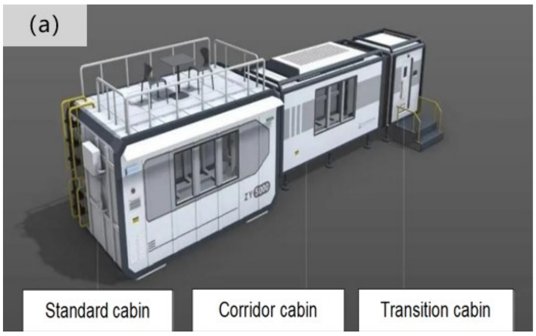

(a) Schematic diagram of the modular cabin configuration of the pressurized cabin

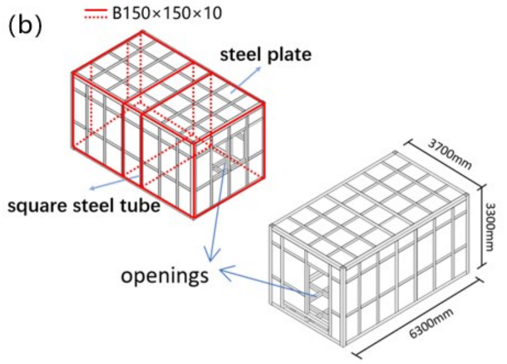

(b) Schematic diagram of the primary structural frame of the pressurized cabin.

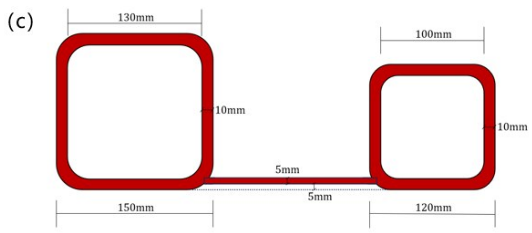

(c) Schematic diagram of the steel tubes in the primary structural frame.

Fig. 2　Diagram of a standard HAHPB cabin and its components(a)

Table 2　Fire resistance rating requirements for building elements

Building element	Fire resistance rating requirements(h)
Primary structural frame	1
Bearing wall	1
Floor construction and associated secondary structural members	1

3.2　FRR requirements

Section 5 of the IBC categorizes buildings of different types based on their height, number of stories, and area. HAHPBs are classified as Type V, Class A based on their height, area, and presence of automatic sprinkler systems, as shown in Table 1. Table 2 gives the FRR requirements for Type V, Class A. In this study, the FRR requirements for the HAHPB steel cabins of interest are 1 hour. By definition, these steel cabins should resist standard fire exposure for at least one hour.

4　Methodology

4.1　FEM simulation

This study utilizes ABAQUS finite element software for modeling and analysis. The geometric dimensions of the model are shown in Figure 2, and the model itself is divided into thermal analysis and mechanical analysis. The heat transfer process involves conduction, convection, and thermal radiation. During a fire scenario, heat affects the structure through these three modes: thermal radiation, convection transfer heat to the structure's surface, and heat conducted internally within the structure. In the thermal analysis model, DS4 elements are used for both square tubes and steel plates, and ISO-834 thermal convection and radiation conditions are applied to the exposed fire surfaces. In the mechanical model, S4R elements are employed, vertical loads are applied by concentrating loads on reference points, and coupling constraints are set between reference points and nodes in the loading area. The position of the reference point for the vertical load is set at the geometric center of the area formed by the four loading positions of the pressurized cabin, and the loading area is selected as the actual pressure-bearing area of the pressurized cabin. The nodes of the loading area and the reference point are coupled in a distributed manner, so that the resultant force acting on the constrained area is equal to the force applied at the reference point, allowing for relative deformation in the constrained area. Internal pressure is uniformly distributed as pressure load on all internal surfaces. This study references European standards for the thermal and mechanical properties of steel at high temperatures[40]. Initial defects are not considered in the modeling process. The finite element model is depicted in Figure 3.

4.2　FDS simulation

This study uses FDS to simulate fire behavior and temperature distribution inside a pressurized cabin during real fire scenarios. FDS simplifies solid

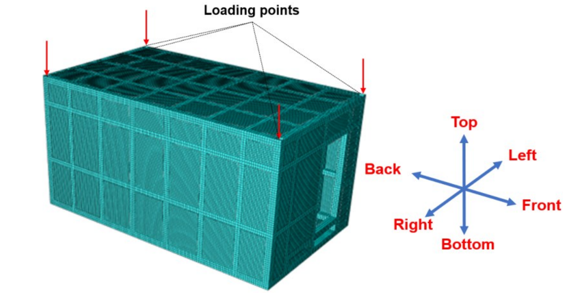

Fig. 3 Standard cabin finite element model

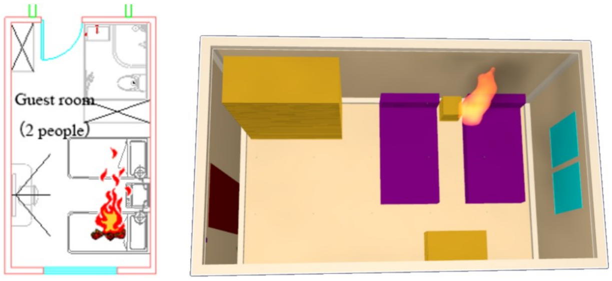

Fig. 4 FDS fire source location diagram

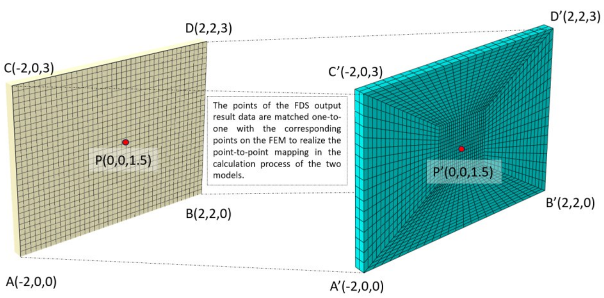

Fig. 5 Coordinate mapping diagram

heat conduction to a one-dimensional process, nd heat transfer within solids is computed using radiation and convective heat flux densities as boundary conditions. Therefore, to obtain a more accurate temperature field of the structure, thermal boundary conditions calculated by FDS are imported into the finite element model for temperature calculation. The simulation first establishes a finite element model and then builds an FDS model based on the coordinates and mesh division of the finite element model. We focus on real room fire scenarios where combustible materials include furniture, mattresses, blankets, and curtains. There are two fire scenarios. One is a simple combustion reaction where the window breaks during the fire, and the other is a complex combustion reaction where the fire self-extinguishes in an enclosed space. Both fire scenarios assume a failure of the sprinkler system while the ventilation system remains operational. The pressurized cabin remains sealed with doors and windows closed during operation. Oxygen replenishment and pressurization are achieved through an oxygen enrichment system and an exhaust gas discharge system, with air being supplied and expelled solely via pipelines. We assume that during operation, both the air intake and exhaust rates of the pressurized cabin are 0.02 m^3/s. In the first fire scenario the fire growth rate coefficient is conservatively estimated to be rapid, with a coefficient of 0.047 kW/s^2. The peak heat release rate, reaching 3.3 MW[45], occurs at 240 seconds and is sustained until the end of the simulation. In the second fire scenario, the fire load is selected as the average value of hotel guest rooms, which is 516.3 MJ/m^2, and the fire source location is set as shown in the Figure 4. The fire originates from the ignited pillow at the head of the bed, which then spreads to surrounding combustible materials.

4.3 FDS-FEM coupling

Our FDS and finite element software differ in their modeling approaches and grid partitioning. The FDS uses a formulation based on low Mach numbers to divide the physical space of fire simulations into numerous rectangular cells for numerical solutions. However, finite element software faces challenges in fully dividing complex geometric models into regular rectangular elements. Additionally, each node in an FDS model does not directly correspond to nodes in a finite element model. Therefore, the coupling method used in this study between FDS and finite element software involves two steps: 1) Mapping the FDS model to the ABAQUS model and 2) Transferring the net heat flux density calculated on the structural surfaces through the FDS model to ABAQUS.

We use NSET-BNDF to output heat flux density from the FDS. Upon successful execution of the FDS model, results are displayed in the form of BNDF files. Using the built-in program fds2ascii, the average heat flux density at each node from the BNDF file during a specific time period is extracted, and the heat flux density data file is output in ASCII format so that it is readable by FE programs. To enhance computational efficiency, we adopt 200 seconds as a time step, using the average heat flux density within this period as the thermal boundary condition for the pressurized cabin. Specifically, the entire simulation period is divided into 200 s intervals. For each interval, the average heat flux calculated by FDS over that period is extracted and applied as the thermal boundary condition on the structural surface in the finite element analysis. Within each time step, the heat flux applied to the structure represents the average value over that interval, which means that the calculated temperature field at the time nodes of each interval is accurate. The heat flux at any instant within the interval is approximated using this average value. Therefore, the choice of the extraction interval does not affect the calculated temperature field at the final time nodes. Subsequently, during the load application step in ABAQUS, modifications are made to the surface heat flux distribution at different positions in the finite element model. By selecting appropriate files from the output database of the surface heat flux distribution module, previously saved ASCII format data files can be effectively retrieved and imported. Ultimately, surface heat flux coupling between the two models is achieved through coordinate mapping. Due to uncertainties in node correspondence, we implement a method of mapping the FDS model to the ABAQUS model based on coordinate indexing. The models are established to maintain consistent shape and size across both software platforms, ensuring complete coordinate alignment between FDS and ABAQUS models, as depicted in Figure 5. The values of the finite element node coordinates are obtained through interpolation using the adjacent coordinate values since the mesh size in the FDS model is typically two to three times larger than that of the FEM model. Each FDS boundary grid represents the area-averaged heat flux over a relatively large surface region. During the mapping process, multiple FEM surface nodes are usually located within a single FDS boundary grid cell. Therefore, the interpolated heat flux values assigned to the FEM nodes generally fall within the spatial resolution already represented by the FDS grid. Since the heat flux density varies relatively smoothly at this scale, the interpolation error introduced during the mapping process can be effectively controlled.

4.4 Validation

The FDS-FEM coupling method has already been well validated against localized fire test data[24,46].

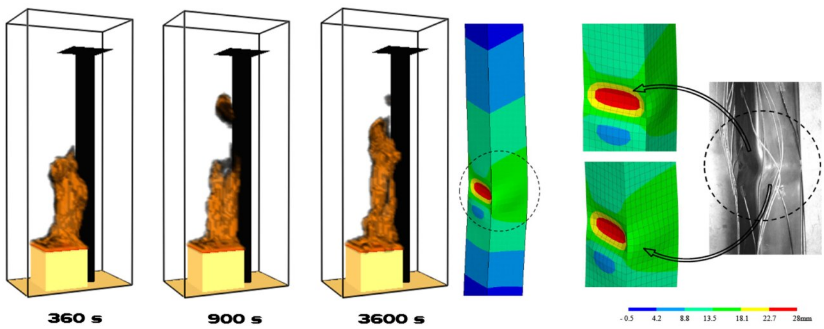

(a) Schematic diagram of displacement distribution and local buckling achieved through thermo-mechanical coupling method

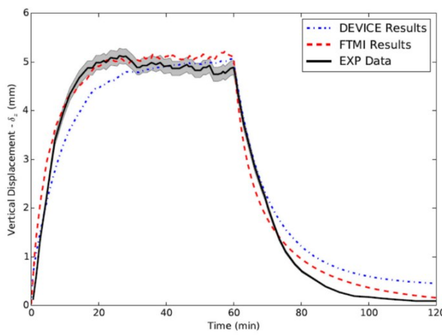

(b) Comparison between measured and predicted vertical displacements in case 1 in Kamikawa et al.'s test

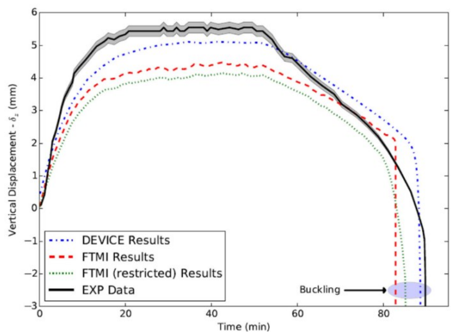

(c) Comparison between measured and predicted vertical displacements in case 4 in Kamikawa et al.'s test

Fig. 6　Modeling localized fire tests on a steel colum[24]

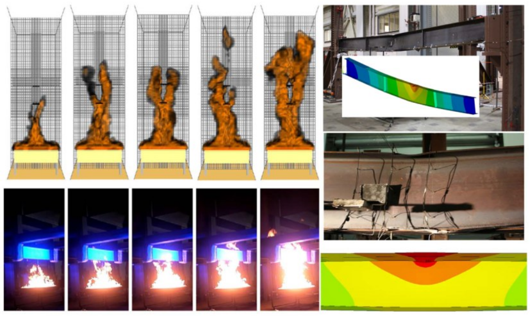

(a) Predicted and measured structural failure mode for the steady test

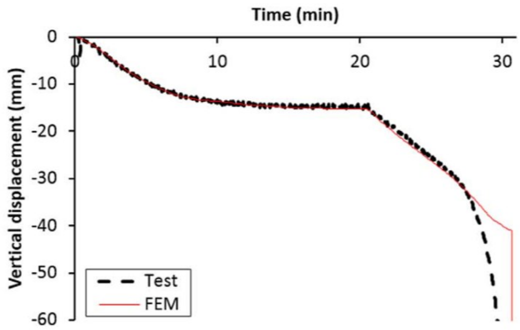

(b) Predicted and measured vertical displacements of the beam specimen for the steady test

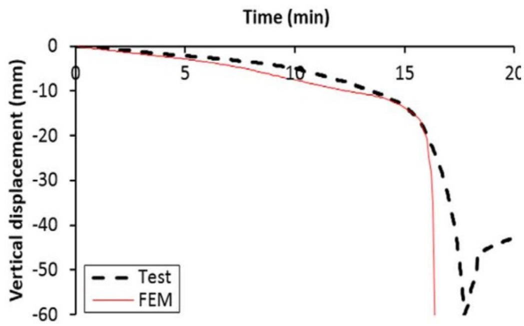

(c) Predicted and measured vertical displacements of the beam specimen for the transient test

Fig. 7 Simulating fire-thermal-structural behavior in a localized fire test on a bare steel beam[46]

5 Analysis and discussion of results

5.1 Failure criteria

As enclosed structures HAHPBs do not have requirements for integrity and thermal insulation. Their load-bearing capacity is considered the sole criterion for FRR. Pressurized cabins, as integral steel frame structures, cannot be subdivided into smaller load-bearing units. However, based on the primary stress forms of each part, each plane forming the cabin enclosure structure can be viewed as an independent load-bearing component. These can be individually evaluated for deformation and deformation rate based on bending and axial load-bearing components.

In the standard fire test[47], a bending component by definition fails when either the bending deformation reaches $L^2/400d$ (mm) or the bending deformation rate reaches $L^2/9000d$ (mm/min). A compression component is by definition failed when either the axial displacement reaches $h/100$ (mm) or the axial displacement rate reaches $3h/1000$ (mm/min). Here L is the clear span of the specimen in mm; d is the distance between the compression and tension points on the cross-section of the specimen in mm; and h is the length of the compression component in mm.

Based on simulation results, it is evident that the internal and external pressure differential is the controlling factor for deformation in the pressurized cabin. The six-sided enclosure primarily resists the bending moments generated by internal pressure. Each side of the enclosure can thus be considered to be a bending component. Conservatively, the maximum section thickness is taken as the distance between the compression and tension points on the specimen cross-section to determine the FRR criteria based on the failure criterion for bending components. The FRR criteria for each structural part are calculated and summarized in Table 3.

The temperature distributions of the pressurized cabin at 1,800s, 3,600s, and 7,200s under standard heating conditions are shown in Figure 8. A temperature-rise curve for 120 minutes is plotted using points A on the cover plate, B on the square steel tube, and C on the top corner of the pressurized cabin, as shown in Figure 9. From these figures we can see that Point A, which is directly exposed to the fire on one side with a plate thickness of only 5mm, experiences the fastest temperature rise. Point B, on the

Table 3 Criteria for failure determination of the cabin

Fire Resistance	Maximum axial compression deformation (mm)	Maximum axial compression deformation rate (mm/min)
Horizontal Structure	192.67	8.56
Vertical Structure	150	6.67
Vertical Structure (Window Side)	187.5	8.33

nonfire-exposed side, experiences a slower temperature rise due to heat conduction and internal cavity radiation. Point C experiences the slowest temperature rise because of the longer heat transfer path.

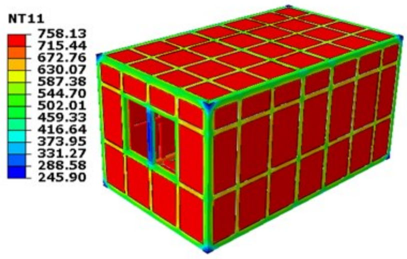

(a) 1 800 s

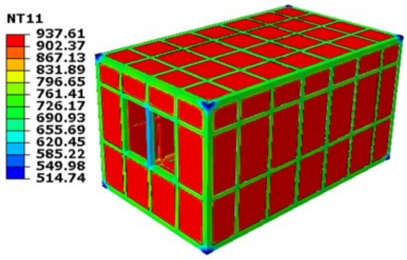

(b) 3 600 s

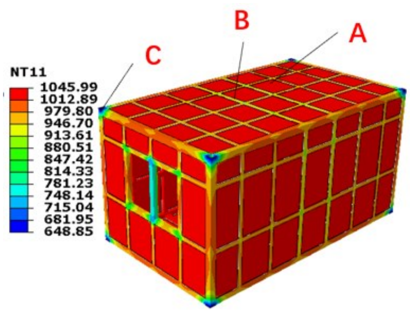

(c) 7 200 s

Fig. 8　Temperature distribution of cabin at 1800s, 3600s, 7200s

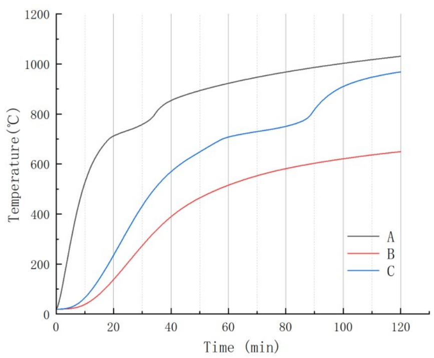

Fig. 9　Time-temperature curves at points A, B, and C

As shown in Figure 10, under an internal and external pressure differential of 0.02 MPa (equivalent to 0.2 atmospheres), and with vertical loads of 200 KN, 500 KN, and 1000 KN applied to the top, the displacement and deformation rates of the six faces of the pressurized cabin are analyzed during a standard 2-hour fire test. At room temperature (20°C), the deformations caused by the internal and external pressure differentials and the vertical loads on the pressurized cabin are negligible compared to those after heating. As the temperature rises, the strength of the steel begins to decrease. In the initial stages, the vertical components deform rapidly, with higher deformation rates compared to horizontal components. This is due to the direct action of the vertical load on the upper end of the vertical components, promoting outward bending deformation of the vertical components. However, as the temperature continues to rise, the deformation rate of the vertical components decreases while that of the horizontal components increases. Around 50 minutes later, the deformation rates of both stabilize, and around 80 minutes later, the displacement of the horizontal components exceeds that of the vertical components. This is because horizontal components have a larger clear span and lower stiffness compared to vertical components, thus exhibiting lower resistance to deformation. From Figure 10, it is evident that an increase in vertical load has a relatively minor impact on the bending deformation of the pressurized cabin at high temperatures. However, it significantly affects the vertical deformation of the vertical components, thereby suppressing thermal expansion deformation in the vertical direction.

According to the FRR criteria calculated in the previous section, the pressurized cabin does not meet the criteria for failure within the standard 2-hour fire test under these three types of horizontal loads. Therefore, its FRR is considered to be greater than 2 hours.

We also obtained the FRR of the pressurized cabin under different internal and external pressure differentials and vertical loads, as shown in Table 4. The load range of 300-1000kN was determined based on preliminary structural design calculations and reference design schemes for typical cabin configurations, representing different numbers of stacked upper compartments. The selected internal-external pressure difference range (0.02-0.05 MPa) is intended to represent the design requirements under varying altitude conditions, including both typical and extreme operating scenarios. Including the design internal pressure of the cabin, the pressure variation associated with changes in external atmospheric pressure at different altitudes, and the safety margins adopted in structural design.

Under consistent internal and external pressure differentials, the influence of vertical loads on the FRR of the pressurized cabin are negligible, indicating that the internal and external pressure differential is the primary factor affecting the FRR.

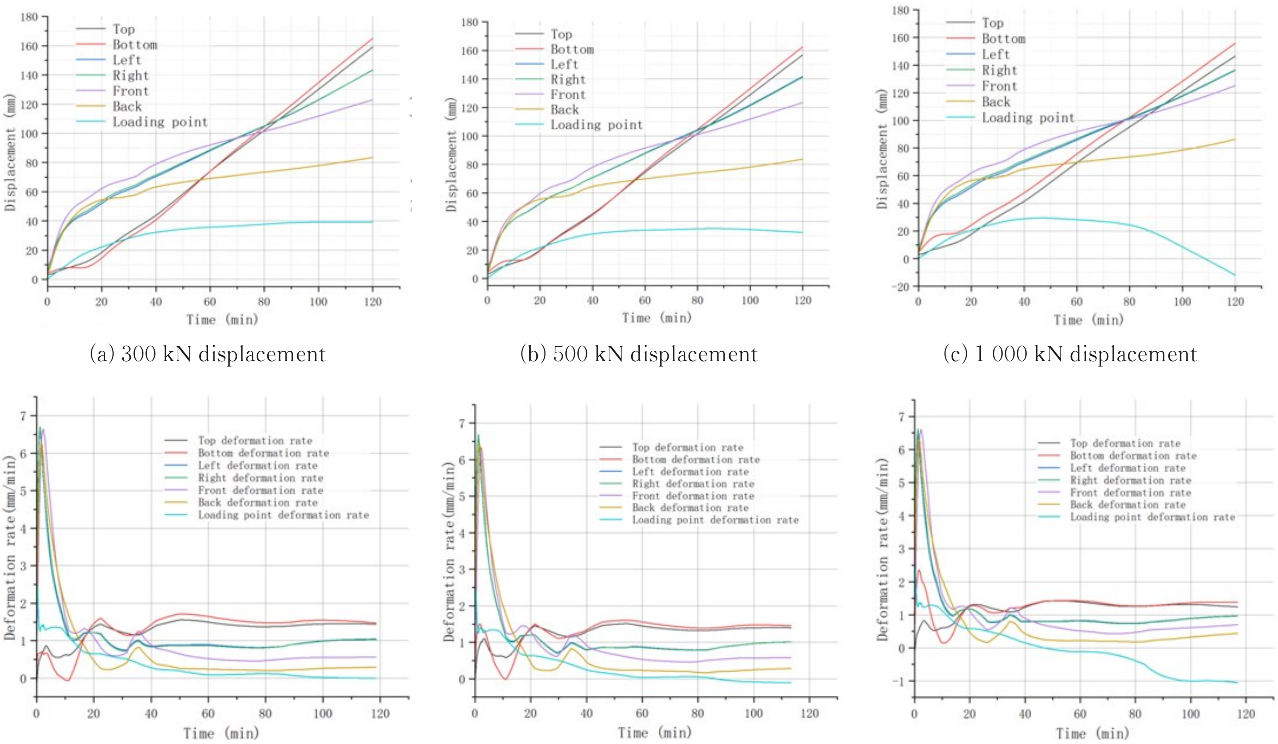

(a) 300 kN displacement (b) 500 kN displacement (c) 1 000 kN displacement

(d) 300 kN deformation rate (e) 500 kN deformation rate (f) 1 000 kN deformation rate

Fig. 10 Time-displacement/deformation rate curves under 0.02MPa pressure differential

Table 4 Fire resistance rating of the cabin under different load levels

Upper vertical load(kN)	Pressure differential 0. 02 MPa	Pressure differential 0. 03 MPa	Pressure differential 0. 04 MPa	Pressure differential 0. 05 MPa
300	＞2h	76 min	58 min	49 min
500	＞2h	76 min	58 min	49 min
1000	＞2h	76 min	58 min	49 min

Table 5 Maximum deformation, stress and temperature of the cabin at different times

Time (min)	Maximum deformation (mm)				Maximum stress (MPa)				Maximum Temperature (℃)
	0. 02MPa	0. 03MPa	0. 04MPa	0. 05MPa	0. 02MPa	0. 03MPa	0. 04MPa	0. 05MPa	
5. 00	36. 01	36. 01	36. 01	40. 63	500. 00	500. 00	500. 00	500. 00	255. 56
10. 00	52. 13	52. 13	52. 13	59. 18	500. 00	500. 00	500. 00	500. 00	491. 49
20. 00	64. 79	64. 79	64. 79	73. 38	500. 00	500. 00	500. 00	500. 00	704. 95
30. 00	69. 97	69. 97	69. 97	106. 80	500. 00	500. 00	500. 00	500. 00	751. 33
40. 00	80. 50	80. 50	80. 50	157. 00	495. 50	495. 50	495. 50	484. 30	848. 99
50. 00	85. 74	85. 74	85. 74	202. 00	428. 40	428. 40	428. 40	410. 60	886. 73
60. 00	92. 98	92. 98	92. 98	261. 90	335. 00	335. 00	335. 00	335. 50	916. 69
80. 00	106. 90	208. 30	274. 20	333. 10	243. 20	246. 70	247. 20	239. 40	961. 63
100. 00	128. 60	259. 90	328. 00	376. 60	194. 80	194. 50	193. 30	194. 20	997. 63
120. 00	155. 90	301. 90	367. 40	417. 40	159. 60	159. 60	159. 60	159. 60	1023. 27

Table 5 also lists the maximum deformation, maximum stress and highest temperature of the pressurization chamber at each time point under different load levels. Since the influence of different vertical loads on the deformation and stress of the pressurization cabin is relatively small, only one vertical load condition of 100kN is listed in the table.

As the pressure differential exceeds 0.02 MPa, the FRR significantly decreases. With further increases in pressure differential, the downward trend in FRR slows down, however. This is because in the initial stages of heating, the steel temperature is not yet high, and its strength is not significantly reduced. Temperature is the primary controlling factor that affects deformation. As the steel temperature rises and its strength decreases, however, the internal and external pressure differential begins to act as the main controlling factor of structural deformation. For pressure differentials between 0.02-0.03 MPa, the pressurized cabin can meet FRR requirements, but for 0.04-0.05 MPa, appropriate fire protection measures are required.

5.3 Analysis of natural fire

A load combination of internal pressure at 0.05 MPa and an upper load of 30 kN was selected for analysis. Figure 11 depicts the temperature distribution within the pressurized cabin after 60 minutes of a real fire scenario. In this scenario, the glass broke during the early stage of fire development, creating direct connectivity with the external environment and resulting in complete pressure release inside the cabin. From Figure 11, it is evident that the high-temperature area is concentrated directly above the fire source, reaching a maximum temperature of 854℃. The temperature field then radiates outward in a ripple pattern from directly above the fire source. The lowest temperature point located at the bottom corner of the pressurized cabin, furthest from the hottest point, measured 111° C. Temperature-time curves were plotted for six points extracted from the top surface of Figure 11. As shown in Figure 12, point A on the cover directly above the fire source experienced the fastest temperature increase, followed by point C on the adjacent sloped cover. Point B on the square steel tube, not directly exposed to the fire, initially warmed at a slower rate compared to points C and D on the sloped cover. However, as time progressed point B ultimately reached a higher temperature than point D due to heat conduction from neighboring high-temperature areas and cavity radiation. Furthermore, Figure 12 shows that temperatures at points A, C, D, and E stabilized after 30 minutes, while points B and F continued to rise. This is because during the rapid development phase of the fire, hot smoke gases moved upwards in the pressurized cabin, accumulating to form a layer of hot smoke gases at the top, which caused rapid heating of the upper air. Points A, C, D, and E, all located on the top panel were directly exposed to the fire below, resulting in rapid temperature increase. Subsequently, during the stable phase of the fire, the temperature of the upper gas stabilized. Point B primarily absorbed heat through conduction and cavity radiation, hence its slower rate of temperature increase. Point F, located farther from the high-temperature area, took longer to reach thermal equilibrium.

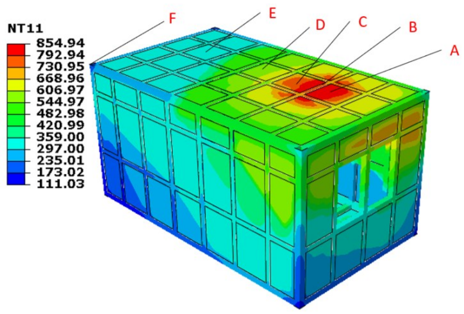

Fig 11 The temperature field of the cabin at 3600s under fire scenario 1

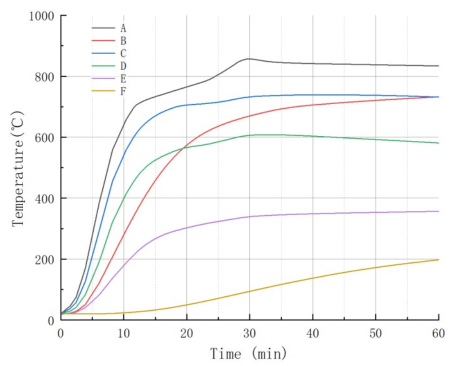

Fig. 12 Time-temperature curves at points A, B, C, D, E, F

Figure 13 depicts stress and displacement contour maps of the pressurized cabin. The corresponding temperature distribution reveals that the high-temperature zone is primarily concentrated in the upper section of the cabin. Due to the window rupture and complete internal pressure release, the cabin structure is subjected only to vertical loading from above, with the low-temperature regions bearing the main structural loads. The maximum deformation of the pressurized cabin occurs in the panel adjacent to the window opening. Due to its relatively thin thickness, the panel undergoes buckling deformation under compressive loading from above. Although the structure maintained integrity for 1 hour without failure according to standard FRR criteria, localized plastic deformation occurred under real fire conditions. This localized deformation may adversely affect the structure's serviceability for post-fire reuse.

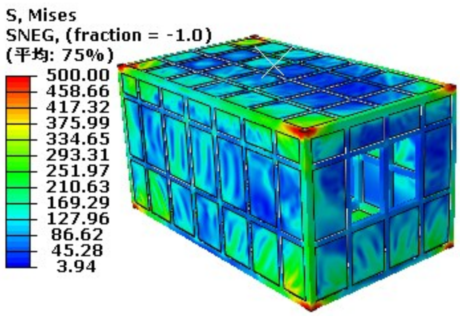

(a) Pressurized cabin stress field

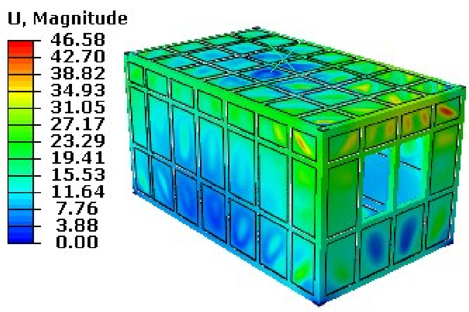

(b) Pressurized cabin displacement field

Fig. 13 Stress and displacement field of the cabin under fire scenario 1

In real fire scenario 2, a fire was initiated in which the fiber material bedding inside the pressurized cabin was ignited. The layout of combustibles and the initial burning state inside the cabin are shown in Figure 4, and the heat release rate (HRR) curve during the fire development is shown in Figure 14. As can be seen from the figure, the HRR reaches its peak at 60 seconds, indicating the fire has become fully developed, with flames spreading throughout the entire room, as illustrated in Figure 16. A total of 16 thermocouples were uniformly distributed on the ceiling of the pressurized cabin to record the temperature-time history of the fire development, as shown in Figure 15. The upper-layer air temperature was relatively uniform and reached its maximum at 60 seconds, which exceeded 1,000 °C. Additionally, the fire and temperature slices at the fully developed stage of the fire are shown in Figure 16. At 62 seconds, the oxygen inside the cabin was completely consumed, and the oxygen supplied through the inlet was insufficient to sustain combustion, as shown in Figure 17. As a result, the fire was rapidly extinguished due to oxygen depletion, with only residual flames continuing to burn near the air inlet.

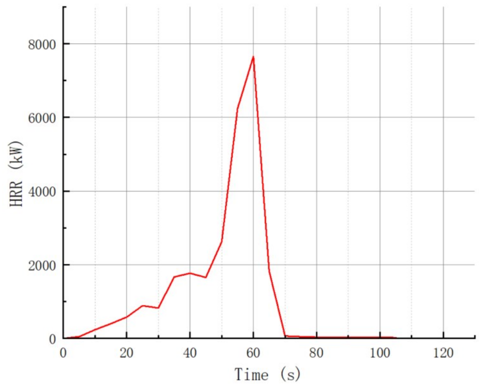

Fig. 14 Heat release rate curve

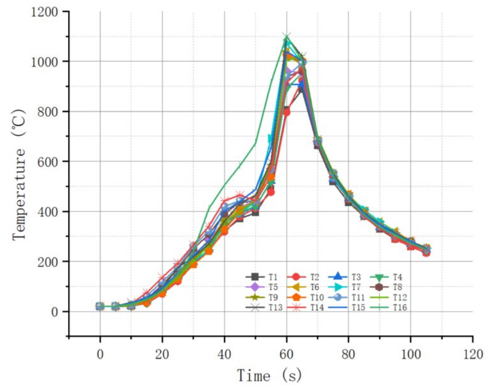

Fig. 15 Ceiling thermocouple temperature curves

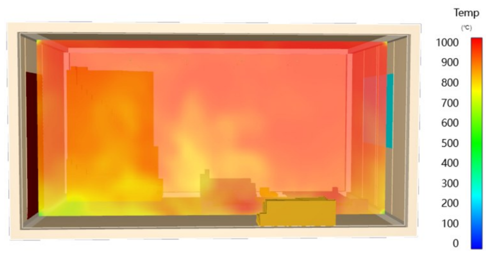

Fig. 16 Fire and temperature slices at the fully developed stage

Although the air temperature inside the cabin was relatively high, the temperature of the pressurized cabin structure was limited due to the short duration of the fire. The peak temperature distribution is shown in Figure 18, with a maximum temperature of

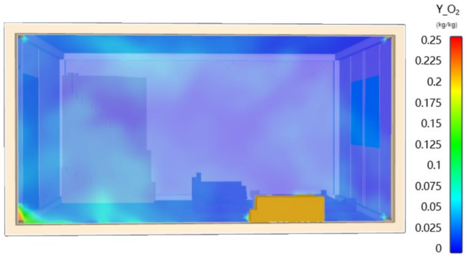

Fig. 17　Oxygen concentration slice at the extinction

232 ˚C occurring near the window. The deformation of the structure was the greatest at this point. A full structural analysis was conducted on the heated pressurized cabin, and the stress and displacement field are shown in Figure 19. The maximum stress occurred at the four upper corners, and it exceeded the yield strength and entering the plastic stage. Due to the moderate temperature of the cabin, the maximum deformation was only 30.9 mm, located in the high-temperature region near the head of the bed, where the wall panel bulged outward under the effect of internal pressure. The overall structure of the pressurized cabin did not undergo significant deformation; only minor, irreversible deformations were observed locally in high-temperature regions.

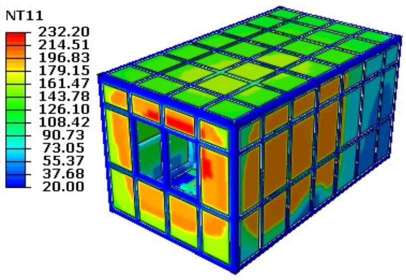

Fig. 18　Maximum cabin temperature under Scenario 2

6　Conclusions

This paper numerically investigated the FR of HAHPBs, a new type of modular construction. By analyzing fire codes from China and the United States, the FRR requirement for steel cabins for the investigated HAHPB is taken to be 1 hour. Numerical simulations were conducted to study the thermo-mechanical responses of an HAHPB steel cabin subjected to both a standard fire and a realistic fire, which included window breakage. Based on this we make the following conclusions, enumerated below.

1) The FR of an HAHPB steel cabin is dependent on the applied pressure level. Under an internal pressure of 0.02 MPa, the FRR of the investigated steel cabin exceeded 2 hours but was reduced to 76 min under pressure of 0.03 MPa. Under pressure of 0.04 MPa, the FRR was less than 1 h.

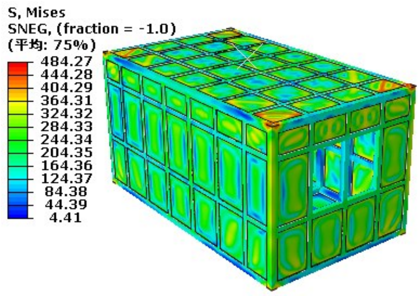

(a) Pressurized cabin stress field

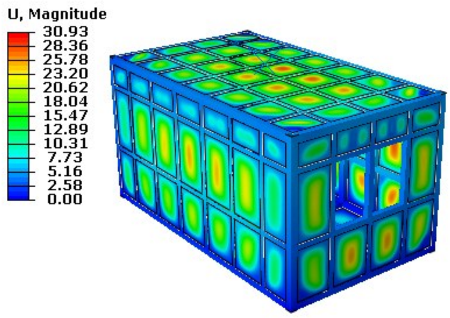

(b) Pressurized cabin displacement field

Fig. 19　Stress and displacement field of the cabin under fire scenario 2

2) Under realistic fire conditions with and without window breakage, the steel cabin maintained its stability during the entire fire period. Note that the measured upper layer gas temperature reached 1,000 ℃ at 60 s for the intact window case, much higher than the case with window breakage.

3) Although the calculation based on the standard ISO 834 requires applying fire protection, the calculation based on the realistic fire did not necessarily warrant it. This highlights the necessity of conducting realistic fire tests to validate calculation results and further develop design guidelines for HAHPB fire safety.

References

[1] China Construction Three Bureau, "Zero Altitude House "let you conquer the Tibetan Plateau[EB/OL]. https://www.thepaper.cn/newsDetail_forward_14861137. (in Chinese)

[2] Li G Q, Han L H, Lou G B. Fire resistance design of steel structure and steel-concrete composite structure [M]. Beijing: China Architecture & Building Press, 2006. (in Chinese)

[3] Lie T T, Lin T D, Allen D E, et al. Fire resistance of

reinforced concrete columns: 1167[R]. Division of Building Research, 1974.

[4] Dotreppe J C, Franssen J M, Bruls A, et al. Experimental research on the determination of the main parameters affecting the behaviour of reinforced concrete columns under fire conditions[J]. Magazine of Concrete Research, 1997, 49(179): 117-127.

[5] Lie T T, Celikol B. Method to calculate the fire resistance of circular reinforced concrete columns[J]. ACI Material Journal, 1991, 88(1): 84-91.

[6] Huang Z F, Tan K H, Phng G H. Axial restraint effects on the fire resistance of composite columns encasing I-section steel[J]. Journal of Constructional Steel Research, 2007, 63(4): 437-447.

[7] Han L H, He J L, Wu H J. Experimental study on fire resistance of concrete filled steel tubular columns[J]. China Civil Engineering Journal, 2000, 33(3): 31-36. (in Chinese)

[8] Li G Q, Zhou H Y. Experimental study on the fire-resistance of steel-concrete composite beams[J]. China Civil Engineering Journal, 2007, 40(10): 19-26. (in Chinese)

[9] Kirby B R. The behaviour of a multi-storey steel framed building subject to fire attack-experimental data[R]. United Kingdom: British Steel Swinden Technology Centre, 1998.

[10] Wu B, Jing Y T. Experimental study on RC space frames with specially-shaped columns subjected to elevated temperature[J]. Journal of South China University of Technology (Natural Science Edition), 2009, 37(6): 129-135. (in Chinese)

[11] Guo S X, Li G Q. Behavior of restrained steel beams subjected to fire and practical fire-resistant design method [J]. Building Structure, 2005, 35(12): 59-61. (in Chinese)

[12] Wang Y C. Steel and composite structures[M]. London: Spon Press, 2002.

[13] Zhang C, Li G Q. FDS simulation of temperature elevation of steel members exposed to large space fire[J]. Journal of Disaster Prevention and Mitigation Engineering, 2012(S1): 68-71. (in Chinese)

[14] Shi J Y, Sun X, Liu W L, et al. Study of performance-based fire resistance design methodology for large space structures[J]. China Civil Engineering Journal, 2011, 44 (5): 69-78. (in Chinese)

[15] Zhang C, Gross J L, McAllister T P. Lateral torsional buckling of steel W-beams subjected to localized fires[J]. Journal of Constructional Steel Research, 2013, 88: 330-338.

[16] Zhang C, Gross J L, McAllister T P, et al. Behavior of unrestrained and restrained bare steel columns subjected to localized fire[J]. Journal of Structural Engineering, 2015, 141(10): 04014239.

[17] Zhang C, Li G Q, Usmani A. Simulating the behavior of restrained steel beams to flame impingement from localized-fires[J]. Journal of Constructional Steel Research, 2013, 83: 156-165.

[18] GB 50016—2014 Code for fire protection design of buildings[S]. (in Chinese)

[19] GB 55037—2022 General code for fire protection of buildings and constructions[S]. (in Chinese)

[20] DB11/ 1740—2020 Design code for residential buildings [S]. (in Chinese)

[21] ICC IBC-2000 International Building Code, 2000[S].

[22] McGrattan K B, McDermott R J, Weinschenk C G, et al. Fire dynamics simulator user's guide[M]. 6th ed. Maryland: National Institute of Standards and Technology, 2014.

[23] Banerjee D K. A software independent tool for mapping thermal results to structural model[J]. Fire Safety Journal, 2014, 68: 1-15.

[24] Zhang C, Silva J G, Weinschenk C, et al. Simulation methodology for coupled fire-structure analysis: modeling localized fire tests on a steel column[J]. Fire Technology, 2016, 52(1): 239-262.

[25] Duan J T, Shi D D, Wang J H, et al. A study of thermal-mechanical coupled method of analyzing steel structures' thermal response in fire based on FDS-ABAQUS[J]. Engineering Mechanics, 2017, 34(2): 197-206. (in Chinese)

[26] Chen Q P, He Y P, Wang X H, et al. Flash point and fire hazard analysis of three organic fuels and their aqueous solutions at low pressures[J]. Fire and Materials, 2018, 42(7): 805-815.

[27] Wu Z B, Zhou X D, Liu X Q, et al. Investigation on the dependence of flash point of diesel on the reduced pressure at high altitudes[J]. Fuel, 2016, 181: 836-842.

[28] Ding C, He Y P, Yin J S, et al. Study on the pressure dependence of boiling point, flashpoint, and lower flammability limit at low ambient pressure[J]. Industrial & Engineering Chemistry Research, 2015, 54(6): 1899-1907.

[29] Ji J, Guo F Y, Gao Z H, et al. Effects of ambient pressure on transport characteristics of thermal-driven smoke flow in a tunnel[J]. International Journal of Thermal Sciences, 2018, 125: 210-217.

[30] Zhang N, Tan Z S. Numerical simulation study on smoke distribution of fire in high-altitude super-long railway tunnels[J]. China Safety Science Journal, 2013, 23(6): 52-57. (in Chinese)

[31] Delichatsios M A. Piloted ignition times, critical heat fluxes and mass loss rates at reduced oxygen atmospheres [J]. Fire Safety Journal, 2005, 40(3): 197-212.

[32] Hirsch D, Williams J, Beeson H. Pressure effects on ox-

ygen concentration flammability thresholds of polymeric materials for aerospace applications[J]. Journal of Testing and Evaluation, 2008, 36(1): 69-72.

[33] Fereres S, Lautenberger C, Fernandez-Pello C, et al. Mass flux at ignition in reduced pressure environments [J]. Combustion and Flame, 2011, 158(7): 1301-1306.

[34] Fereres S, Lautenberger C, Fernandez-Pello A C, et al. Understanding ambient pressure effects on piloted ignition through numerical modeling[J]. Combustion and Flame, 2012, 159(12): 3544-3553.

[35] Qie J F, Yang L Z, Wang Y F, et al. Experimental study of the influences of orientation and altitude on pyrolysis and ignition of wood[J]. Journal of Fire Sciences, 2011, 29(3): 243-258.

[36] Zhang C, Li G Q. Response of steel members subject to temperature gradient in localized fires [C]//Fire Science and Technology 2015. Singapore: Springer, 2017: 309-317.

[37] Usmani A S, Rotter J M, Lamont S, et al. Fundamental principles of structural behaviour under thermal effects [J]. Fire Safety Journal, 2001, 36(8): 721-744.

[38] Tan K H, Yuan W F. Buckling of elastically restrained steel columns under longitudinal non-uniform temperature distribution[J]. Journal of Constructional Steel Research, 2008, 64(1): 51-61.

[39] Scullion T, Ali F, Nadjai A. Experimental study on performance of elliptical section steel columns, under hydrocarbon fire[J]. Journal of Constructional Steel Research, 2011, 67(6): 986-991.

[40] DS/EN 1993-1-2: 2024 Eurocode 3 - Design of steel structures - Part 1-2: Structural fire design[S].

[41] Agarwal A, Choe L, Varma A H. Fire design of steel columns: Effects of thermal gradients[J]. Journal of Constructional Steel Research, 2014, 93: 107-118.

[42] Yin Y Z, Wang Y C. Numerical simulations of the effects of non-uniform temperature distributions on lateral torsional buckling resistance of steel I-beams[J]. Journal of Constructional Steel Research, 2003, 59(8): 1009-1033.

[43] Dwaikat M M S, Kodur V K R, Quiel S E, et al. Experimental behavior of steel beam-columns subjected to fire-induced thermal gradients[J]. Journal of Constructional Steel Research, 2011, 67(1): 30-38.

[44] Possidente L, Couto C, Tondini N, et al. Review of design approaches for steel columns subjected to localised fires: Insights from the 2nd generation Eurocode model [J]. Engineering Structures, 2024, 315: 118424.

[45] Yuan J P, Li S J, Zhang K, et al. Fire behavior in a hermetic pressurization building for reducing the effects of high altitude: a case study[J]. Fire, 2023, 6(5): 178.

[46] Zhang C, Yu H X, Choe L, et al. Simulating the fire-thermal-structural behavior in a localized fire test on a bare steel beam[J]. Engineering Structures, 2018, 163: 61-70.

[47] ISO 834-1: 2025 Fire-resistance tests - Elements of building construction - Part 1: General requirements[S].

（编辑　XXX）